Applied Catalysis B: Environmental 244 (2019) 881–888

Contents lists available at ScienceDirect

Applied Catalysis B: Environmental

journal homepage: www.elsevier.com/locate/apcatb

Covalent ligation of Co molecular catalyst to carbon cloth for efficient electroreduction of CO_2 in water

Aleksei N. Marianov, Yijiao Jiang*

School of Engineering, Macquarie University, Sydney, NSW, 2109, Australia

ARTICLE INFO

Keywords:
CO_2 electroreduction
Electrochemistry
Covalent immobilization
Cobalt porphyrin

ABSTRACT

Electrochemical reduction of CO_2 to CO in water catalysed by porphyrins is a viable way to environmentally friendly CO_2 valorisation, while efficient catalyst immobilization on the electrode surface is one of the key challenges to answer. Herein we present a concept of "molecular wire" i.e. connection of the catalyst to electrode via a conductive covalent linker. To covalently immobilize Co porphyrin core onto carbon cloth we employed reduction of corresponding diazonium salt. "Wiring" via resulting phenylene group had profound effect on electrocatalytic performance. Formation of CO in neutral aqueous electrolyte at –1.05 V vs NHE (η = 500 mV) occurs with TOF of 8.3 s^{-1} while noncovalent counterpart has TOF of 4.5 s^{-1} only. Compared to the noncovalent mode, covalent ligation leads to 2.4 times higher surface density of electrochemically active species and maximum FE (CO) is achieved at 50 mV less negative potential. The catalyst accumulated $3.9{\cdot}10^5$ TON in 24 h long electrolysis surpassing performance of drop-cast analogue by a factor of 3 and showed FE (CO) of up to 81%. Notably, the TON and TOF values achieved in our study are one of the highest reported to date surpassing those measured for Fe hydroxyporphyrins and Co porphyrin-based covalent organic frameworks. Electrokinetic analysis demonstrated that the electron transfer from electrode onto porphyrin moiety plays an important role in overall reaction kinetics and conductive link with the support is a key element of heterogeneous catalyst design.

1. Introduction

Carbon dioxide (CO_2) is an abundant single-carbon compound which has enormous industrial potential. To bring about its use as a raw material, efficient and environmentally friendly valorisation methods must be developed. CO_2 electrochemical reduction reaction (CO_2ERR) in aqueous medium is one of the most promising approaches allowing to produce value-added products such as CO and formate [1–5]. To minimize energy losses in this process, the anion radical formed upon first one-electron reduction has to be stabilized on electrocatalyst thus forcing the reaction through a less demanding proton coupled multi-electron pathway [6–8]. A wide range of materials including metals [9,10], metal oxides [11], metal sulfides [12], carbon-based composites [13–15] and organometallic compounds [8] has been reported to be capable of lowering CO_2ERR overpotential.

Among organometallics, stable and readily accessible porphyrin and structurally similar phtalocyanine complexes of first row transition metals combine high TOF and versatility of fine structure tuning. Over the course of the past four decades numerous potent homogeneous catalysts were discovered [16–21] and reaction mechanisms were elucidated [22–30]. However, cumbersome catalyst recycling and use of organic solvents limit feasibility of homogeneous systems. Thus, it was recognized that the development of heterogeneous organometallic electrocatalysts operating in aqueous electrolytes is necessary to combine simplified recovery of solid materials and outstanding activity of homogeneous catalysts [31].

Generally, heterogenization could be achieved with and without creation of a direct chemical bond between the catalyst and the support. Noncovalent electrode modification is the simplest approach allowing to quickly immobilize complex on the electrode surface via drop-casting. As such, high activity of Co tetraphenylporphyrin (CoTPP) and Co phtalocyanine composites with carbon nanotubes (CNT) rely on high surface area of CNT to maximize CO_2 reduction activity [32,33]. Pyrene-appended Fe porphyrin makes use of π-π interactions between CNT carbon plane and its pyrene unit [34]. Approaches based on incorporation of porphyrin core into metal-organic frameworks (MOFs) [35,36] and covalent organic frameworks (COFs) [37,38] produced good catalysts with the latter yielding TON of up to $2.9{\cdot}10^5$ with overpotential 550 mV. Notwithstanding their utility, noncovalently immobilised catalysts may suffer from slow electron transfer and leaching due to weak connection to the electrode [34,39].

In turn, covalent attachment is rather appealing option since a

* Corresponding author.
E-mail address: yijiao.jiang@mq.edu.au (Y. Jiang).

https://doi.org/10.1016/j.apcatb.2018.11.084
Received 7 September 2018; Received in revised form 21 November 2018; Accepted 28 November 2018
Available online 28 November 2018

catalyst could be tethered to the electrode via stable chemical bond assuring fast electron transfer onto catalytically active centre and protecting material against physical damage in the conditions of severe effervescence. However, reports of covalently immobilised CO_2ERR catalysts are much scarcer due to more sophisticated preparation and so far, TONs/TOFs reported for covalently tethered complexes have been quite low. As such, Fe hexahydroxyporphyrin was grafted to carbon nanotubes via amide linker accumulating TON of 532 over 3 h in aqueous electrolyte at −1.06 V vs NHE [40]. In another example, Co porphyrin was attached to conductive diamond via long 1,2,3-triazolyl-terminated alkyl chain. This hybrid electrode maintained CO_2 reduction current after 10^3 cycles between -0.5 and -1.8 V vs Ag/Ag^+ in acetonitrile [41]. CO formation was unambiguously detected by FTIR; however, no TON was experimentally measured. The third example is covalent grafting of Co terpyridine onto glassy carbon with the following study of its activity in hydrogen evolution reaction and CO_2ERR in DMF [42]. Although in the presence of CO_2 faradic current dropped to the baseline levels within 30 min, the catalyst showed TON in CO of 70. Notably, potentially explosive pure diazoniums salts have often been used as grafting agents [40–43].

In the present work, we endeavored to attach covalently CoTPP to the surface of carbon cloth via phenylene linker using electroreduction of the corresponding diazonium salt safely generated in situ. We assumed such a short conductive linker would enhance rate of electron transfer onto Co centre, impart higher stability to the resulting material and increase surface concentration of electrochemically active complex [44]. Indeed, the number of catalytically active moieties considerably increased, TOF at overpotentials below 550 mV greatly improved as well while electrokinetic analysis proved the crucial importance of covalent linker as it facilitated electron transfer onto Co porphyrin centre. As a result, the hybrid material showed much higher activity in CO_2ERR during 24 h long electrolysis and outperformed the popular Fe hydroxyporphyrin analogues [34,40].

2. Experimental

2.1. Chemicals and materials

Chemicals were purchased from Sigma Aldrich and Alfa Aesar. Benzaldehyde and pyrrole were distilled under reduced pressure before use. Tetrabutylammonium hexafluorophosphate (TBAP) was recrystallised from ethanol and dried at 110 °C. Anhydrous *N,N*-dimethylformamide (DMF) over molecular sieves was obtained from Ajax Finechem (purity > 99.9%; moisture content < 100 ppm). Two-compartment electrochemical H-cell was purchased from Pine Research Instrumentation. Carbon cloth was bought from Fuel Cell Store. Flash column chromatography was performed on silica gel 70–230 mesh. Syntheses of tetraphenylporphyrin, TPP-NH_2 and CoTPP are described in SI.

2.2. Preparation of CoTPP-cov and CoTPP-noncov

Carbon cloth was washed with concentrated HCl, trifluoroacetic acid (TFA) and water, cut into 1*5 cm rectangular pieces, sewed with 0.5 mm silver wire through the one end, sealed with melted polypropylene to leave another end free and used as a working electrode.

CoTPP-cov was prepared as follows: 5-(4-aminophenyl)-10,15,20-triphenylporphyrin **TPP-NH_2** (15.1 mg, 0.024 mmol) was dissolved in 6 mL of H_2O:TFA (1:1) mixture and cooled down to −5 °C on an ice-salt bath under the mild flow of inert gas. $NaNO_2$ (248.4 mg, 3.6 mmol) was dissolved in 10 mL of deionized water and 100 µL aliquot (1.5 eqv) was added into the reaction flask dropwise with the following stirring for 1 h. Septum with three electrodes was placed on top, electrodes were soaked in the solution for 30 min and the potential of 0.0 V vs Ag/AgCl (3 M KCl) was applied for 1 min. Working electrode was removed, thoroughly washed with ethanol, DMF, water and dried at 80 °C for 3 h. Porphyrin-modified electrodes were soaked at 0.05 M $Co(OAc)_2$ solution in DMF:CH_3COOH (9:1) at 120 °C for 45 min, then washed with DMF, water and used fresh in catalytic experiments.

CoTPP-noncov was prepared by dropping of 2 mM CoTPP solution in DMF onto clean, dry carbon cloth electrodes with the following drying at 80 °C for 3 h. Electrodes were washed with deionised water before catalytic experiments.

2.3. Electrochemical measurements

All electrochemical measurements were conducted on BioLogic SP-300 potentiostat using Ag/AgCl (3 M KCl) reference electrode and Pt coil as an auxiliary electrode. 25 mL flask was used as a single-compartment electrochemical cell for all cyclic voltammetry measurements. CVs in DMF were performed using non-aqueous reference electrode (Ag wire immersed in DMF solution of 0.05 M $AgNO_3$ and 0.1 M TBAP) calibrated against Fc^+/Fc redox couple [45]. Controlled potential electrolyses were performed in a two-compartment H-cell with cathodic and anodic spaces separated by porous glass frit and ground joints on top. Electrode wires were passed through the thick rubber septa fitted on top of the cell to assure gas-tight seal. Gaseous products from the cathodic headspace were analysed on GC 2014 (Shimadzu) equipped with a packed Restek 6 ft column (molecular sieves 5 Å, i.d. 2 mm) and TCD detector. Helium was used as a carrier gas. Water discharge current was calculated via subtraction of CO_2ERR partial current from the total value.

2.4. Estimation of the complex electrochemically active surface loading

Electrochemically active surface loading (Γ_{EA}, mol/cm^2) was calculated from integration of Co^{II}/Co^{I} reduction wave using Eq. (1): [46]

$$\Gamma_{EA} = \frac{Q_{CV}}{nFA} \quad (1)$$

Where Q_{CV} – charge determined via integration of Co^{II}/Co^{I} reduction peak (C), n – number of electrons transferred (1 in this case), F – Faraday's constant (96,485 C/mol), A – electrode area (cm^2).

Complimentary method of calculation was employed using Eq. (2) to validate Γ_{EA} estimation: [46]

$$\Gamma_{EA} = \frac{4i_pRT}{F^2A\nu} \quad (2)$$

Where i_p – peak reoxidation current of Co^{II}/Co^{I} reduction wave (A), R – universal gas constant (8.314 J/(mol K), T – electrolyte temperature (296 K), ν – potential scan rate (V/s)

2.5. Determination of TON, TOF and FE (CO)

Turnover numbers (TON) and turnover frequencies (TOF) in CO were determined using Eqs. (3) and (4), respectively:

$$TON = \frac{(CO)_i}{\Gamma_{EA}A} \quad (3)$$

$$TOF = \frac{(CO)_i}{\Gamma_{EA}A\tau} \quad (4)$$

Where $(CO)_i$ – amount of CO measured with GC at a given time i (mol), τ – reaction time (s). Faradic efficiency [FE (CO)] values were calculated from the Eq. (5):

$$FE_{CO} = 100\frac{[(CO)_i - (CO)_{i-1}]nF}{(Q_i - Q_{i-1})} \quad (5)$$

2.6. Characterisation methods

JEOL JSM 7100 F FESEM microscope was used for SEM imaging and

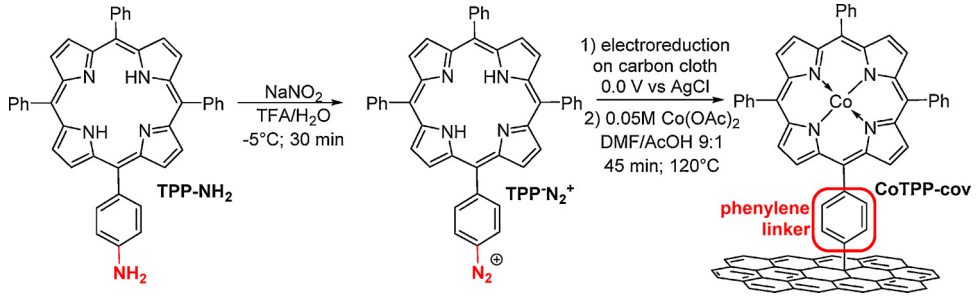

Scheme 1. Preparation of covalently immobilised Co tetraphenylporphyrin (**CoTPP-cov**).

EDS was performed on PHENOM XL Benchtop SEM. Raman spectra were recorded on Lab RAM HR Evolution spectrometer using 473 nm laser. For representative Raman studies the top areas of carbon fibres were analysed to assure 90° angle between laser beam and the surface under investigation.

3. Results and discussion

3.1. Immobilisation of CoTPP on carbon cloth

Covalently immobilised Co tetraphenylporphyrin (**CoTPP-cov**) was prepared using multistep procedure as described in the Scheme 1. Diazotation of **TPP-NH$_2$** in aqueous trifluoroacetic acid (1:1) at −5 °C generates **TPP-N$_2$**$^+$ and the following electroreduction at 0.0 V vs Ag/AgCl (3 M KCl) in potentiostatic mode on carbon cloth electrode furnishes layer of covalently grafted porphyrin [47–50]. Introduction of cobalt atom into surface-tethered porphyrin core was attained via treatment with 0.05 M solution of $Co(OAc)_2$ in DMF/CH_3COOH (9:1) at 120 °C with the formation of hybrid material **CoTPP-cov** [51]. Scanning electron microscopy (SEM) study revealed lack of visible crystalline deposits and only scattered thin patches of polymerized material could be seen (Fig. 1a). Energy dispersive X-ray spectroscopy (EDS) mapping shows uniform distribution of nitrogen and Co throughout the surface of carbon fibers confirming good coverage with Co porphyrinate (Fig. 1b). Also, we believe that rather positive potential used for grafting allowed to mitigate overreduction of transient radicals and achieve their connection with the carbon surface [43,50].

To compare properties of the same catalyst in noncovalent immobilisation mode we prepared electrodes via drop-casting of CoTPP solution in DMF onto carbon cloth (denoted as **CoTPP-noncov**). The total amount of deposited complex was $8{\cdot}10^{-8}$ mol/cm^2 unless otherwise noted.

Electrochemical and Raman studies were performed to confirm the formation of covalently immobilised porphyrin layer. Cyclic voltammetry (CV) in dry oxygen-free DMF containing 0.1 M of tetrabutylammonium hexafluorophosphate (TBAP) as supporting electrolyte (Fig. 1c, red trace) showed typical responses of Co^{II}/Co^{I} and Co^{I}/Co^{0} redox pairs at -1.30 V and -2.39 V vs Fc^+/Fc respectively. These values are close to the formal redox potentials of $[Co^{II}TPP]/[Co^{I}TPP]^-$ and $[Co^{I}TPP]^-/[Co^{0}TPP]^{2-}$ in homogeneous solution (- 1.31 and 2.42 V vs Fc^+/Fc, Fig. 1c, blue trace). Covalent nature of the complex immobilisation could be inferred from the fact that the **CoTPP-noncov** is easily washed away from the electrode with DMF leaving pristine carbon fabric without any characteristic redox behavior. In turn, removal of electrodeposited complex could not be attained by any means without destruction of the electrode. CV measurements in degassed aqueous 0.5 M KOH gave surface loading of electrochemically active complex (Γ_{EA}) of ~ $6.9{\cdot}10^{-10}$ mol/cm^2 with clear linear correlation between peak current and potential scan rate (Fig. 1d-e). Values of Γ_{EA} found by integration of reduction wave using Eq. (1) and from the reoxidation peak currents through the Eq. (2) are in good agreement.

Raman spectra provided additional evidence of CoTPP formation on the surface (Fig. 1f). Since retention of signature signals is expected upon immobilisation, a band at 385 cm^{-1} found in the spectra of **CoTPP-cov** and **CoTPP-noncov** could be identified as the strongest peak of CoTPP spectrum. [33,52] Notably, both for **CoTPP-noncov** and **CoTPP-cov** the peak is shifted compared to unsupported complex by 9 cm^{-1} and in the latter case is more diffuse. Also, a group of bands corresponding to C—H vibrations between 3000 and 3200 cm^{-1} clearly visible in the spectra of **CoTPP-noncov** and free CoTPP does not appear in the case of **CoTPP-cov** (Fig. 1f). Overall, changes in CoTPP Raman spectra upon attachment to the carbon support could be interpreted as a result of strong electronic interactions with its surface [33,53].

Regarding **CoTPP-noncov**, CV response of reversible redox couple $[Co^{II}TPP]/[Co^{I}TPP]^-$ in degassed 0.5 KOH was also used to calculate Γ_{EA}. Clearly, only $2.9{\cdot}10^{-10}$ mol/cm^2 or 0.36% of all deposited complex is electrochemically active (Fig. 2a). Typical for heterogeneous systems linear dependence of peak current on the potential scan rate is clearly seen and Γ_{EA} calculated by integration of the reduction wave correlates with the value obtained from the peak reoxidation current (Fig. 2b). Representative SEM imaging of the resulting material revealed formation of flaky crystals greatly segregated on the edges of carbon cloth (Fig. 2c, S11). EDS mapping showed high concentrations of cobalt and nitrogen in these aggregates with uniform distribution of these elements across other parts of the surface (Fig. 2c).Clearly, most of the area bears uniformly adsorbed layer of CoTPP while crystals are formed by the material left after surface saturation.

We also estimated average surface area occupied by a single porphyrin unit. Ratio of electrochemically active surface area (S_{EA}) to geometric area (SG) for carbon cloth was found to be 2.6 using double layer capacitance (DLC) measurements as described in SI. Considering Γ_{EA} of $6.9{\cdot}10^{-10}$ mol/cm^2, each porphyrin moiety in **CoTPP-cov** on average takes 0.4 nm^2 while this value for **CoTPP-noncov** is 0.9 nm^2. These values give grounds to believe that we deal with a thin multilayer rather than with a monolayer on the surface of **CoTPP-cov** and **CoTPP-noncov** as well.

Additionally, immobilization mode considerably affects the double layer capacitance. As measured in 0.1 M KOH electrolyte, carbon cloth and **CoTPP-noncov** have DLC of ~ 289 and 219 μF/cm^2, respectively (Figures S9 and S10 respectively). We believe organic film in noncovalent immobilisation mode is quite permeable and it is possible for electrolyte to reach the electrode surface under the layer of complex while 70 μF/cm^2 drop is rather caused by the presence of microcrystals isolating carbon from electrolyte. In turn, DLC of **CoTPP-cov** is 391 μF/cm^2 (Figure S10) which is 102 μF/cm^2 higher than that of bare carbon fabric showing that the electrodeposited layer of hydrophobic porphyrin is quite dense as the capacitance increase comes from the diffusion limitations imposed on solvated ions by organometallic moieties [54].

To sum up, we immobilised Co porphyrin on the surface of carbon cloth in covalent and noncovalent modes. Carbon fibers are uniformly covered with the redox active layer of Co porphyrinate in both cases as clearly evidenced by electrochemical studies and Raman spectra. Covalent ligation of porphyrin core to the surface of carbon cloth could

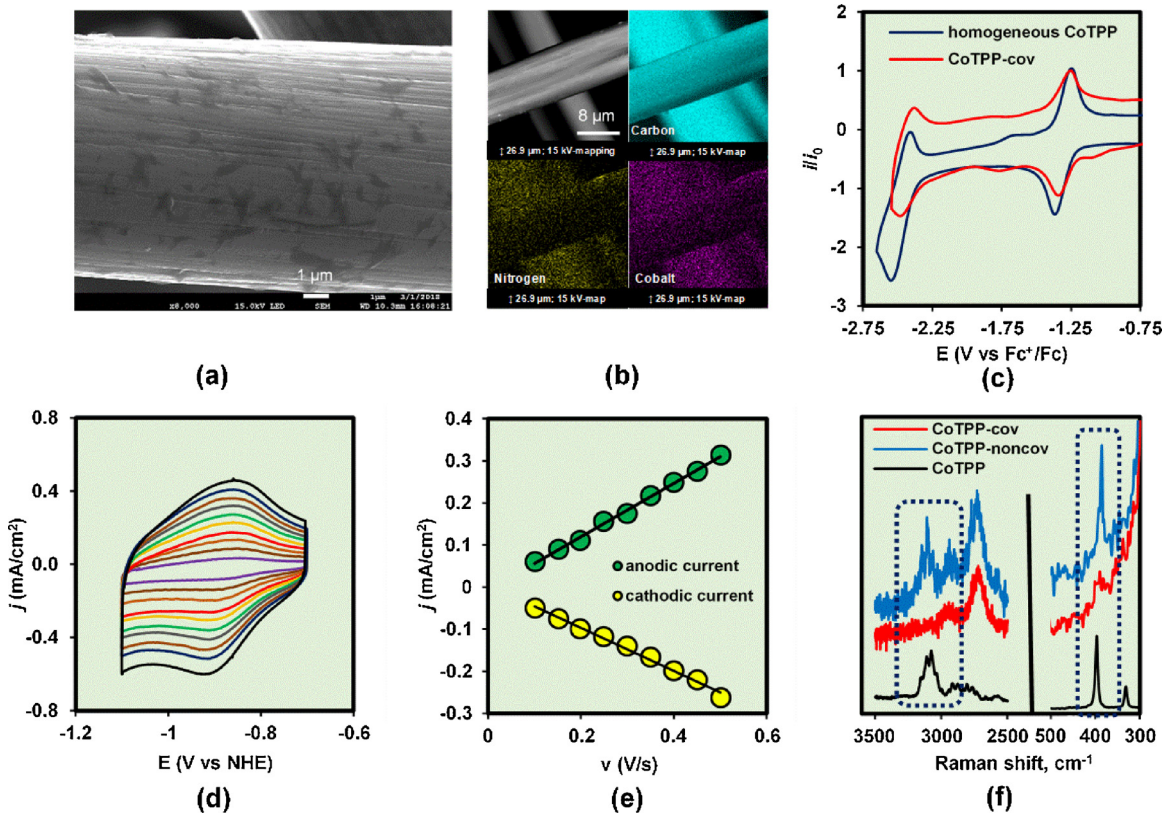

Fig. 1. (a) SEM imaging and (b) EDS mapping of **CoTPP-cov**; elements shown are: C (cyan), N (yellow) and Co (violet). (c) CV of CoTPP and **CoTPP-cov** in DMF containing 0.1 M of TBAP as a supporting electrolyte, scan rate 100 mV/sec, currents are normalized to the Co^{II}/Co^{I} reoxidation peak; (d) dependence of CV shape and (e) peak current density on the potential scan rate in degassed 0.5 M aqueous KOH electrolyte; (f) Raman spectra of **CoTPP-cov**, **CoTPP-noncov** and solid CoTPP. TBAP: tetrabutylammonium hexafluorophosphate. (For interpretation of the references to colour in this figure legend, the reader is referred to the web version of this article).

be inferred from the facts that immobilized complex in **CoTPP-cov** is not soluble in organic solvents and appear to closer interact with carbon fibers than in **CoTPP-noncov** which results in higher DLC capacitance [54]. In the following study we consider values of Γ_{EA} as the active amount of complex taking part in CO_2ERR (Fig. 1c and 2 a).

3.2. Catalytic activity of CoTPP-cov and CoTPP-noncov in aqueous medium

CV was used to assess overall activity of CoTPP in both immobilisation modes. Voltammograms showed poorly defined irreversible reduction peaks heavily overlapped with H^+ discharge (Fig. 3a-b). Characteristic increase of the reduction current and shift of its onset towards more positive potentials upon saturation of the electrolyte with CO_2 were clearly observed as well [38]. As such, for **CoTPP-noncov** in degassed electrolyte the reduction current of 1 mA/cm^2 was attained at -0.99 V vs NHE while in the presence of CO_2 the same value was reached at -0.92 V (Fig. 3a). Comparison of **CoTPP-noncov** and **CoTPP-cov** shows that overall activity of the latter is considerably higher. As measured at -1.0 V, faradic current in CO_2-saturated electrolyte rose from 1.7 to 4.7 mA/cm^2 with the introduction

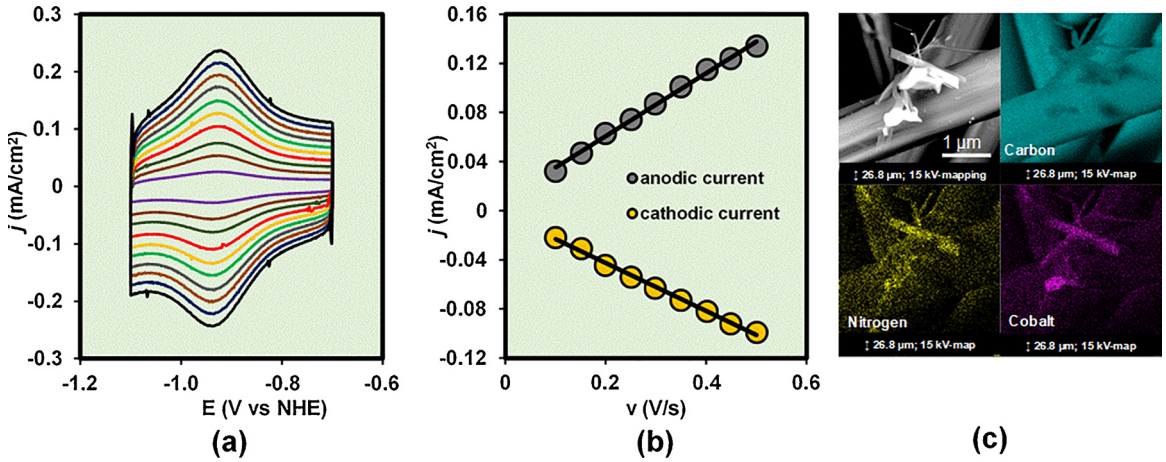

Fig. 2. (a) CV of **CoTPP-noncov** on carbon cloth electrode and (b) anodic and cathodic peak currents of Co^{I}/Co^{II} redox pair in 0.5 M degassed KOH at various scan rates; (c) SEM image and EDS mapping of **CoTPP-noncov.**

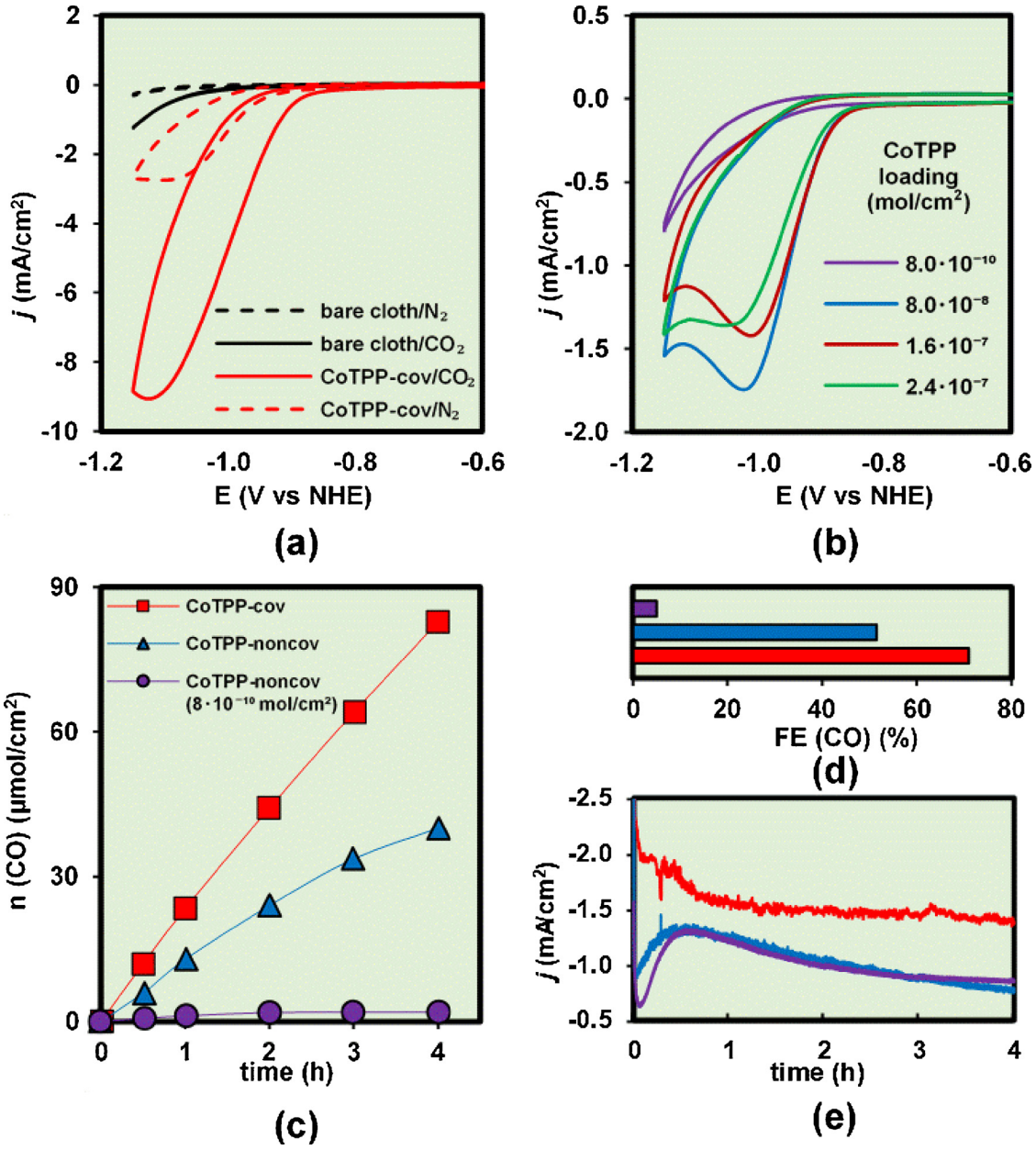

Fig. 3. (a) CVs of **CoTPP-cov** in N_2- and CO_2-purged aqueous electrolyte, CVs of bare carbon cloth are shown for clarity; (b) CV traces of **CoTPP-noncov** with the variable amount of noncovalently immobilised CoTPP in CO_2-saturated electrolyte; (c) total amount of CO, (d) FE (CO) and (e) current densities observed during 4 h long controlled potential electrolyses (CPE) at -1.10 V vs NHE in CO_2-saturated electrolyte. Electrolyte: 0.5 M $KHCO_3$ in all cases, potential scan rate is 100 mV/s.

of covalent link (Fig. 3a, red trace and Fig. 3b, blue trace). Interestingly, CV of an electrode bearing $8{\cdot}10^{-10}$ mol/cm^2 of CoTPP (amount is similar to Γ_{EA} of **CoTPP-cov**) was close to the one recorded for bare carbon cloth (Fig. 3b, violet trace). Increase of surface loading to $1.6{\cdot}10^{-7}$ and $2.4{\cdot}10^{-7}$ mol/cm^2 did not improve catalytic activity thus additionally proving saturation of carbon surface with CoTPP (Fig. 3b, green and brown traces, respectively). To confirm results obtained from the analysis of CV curves, 4 h long electrolyses at -1.10 V (η = 550 mV) were undertaken. **CoTPP-cov** exhibited much higher CO production rate of 82 µmol/cm^2 with the FE (CO) of 71% and current density of ~ 1.5 mA/cm^2 while **CoTPP-noncov** produced only 40 µmol/cm^2 of CO with FE (CO) of 52% and current density of ~ 1 mA/cm^2 (Fig. 3c-e, red and blue traces, respectively). In good agreement with CV data, decrease of the complex loading to $8{\cdot}10^{-10}$ mol/cm^2 led to the sharp drop of CO_2 reduction efficiency to 1.9 µmol/cm^2 with FE (CO) of 5% only (Fig. 3c–e, violet traces). Bare carbon cloth also produces 1.7 µmol of CO with FE (CO) of 1.7%, but immobilisation of porphyrin layer almost completely suppresses its activity (Figure S13a).

Encouraged by the results of preliminary evaluation, we performed a series of 30 min electrolyses at the potentials between -1.00 and -1.20 V vs NHE. The aim of this electrokinetic study was to optimize electrode potential in CO_2ERR, gain insight into the influence of covalent bond with the electrode on the reaction mechanism and clarify the nature of active sites responsible for concurrent hydrogen evolution. As clearly seen from Fig. 4a, the total amount of CO produced by **CoTPP-cov** is much higher at all potentials reaching 16.1 µmol/cm^2 at -1.20 V as opposed to **CoTPP-noncov** which yields 7.1 µmol/cm^2 under the same conditions.

Although the better overall CO evolution rate is not surprising considering higher amount of electrochemically active complex in **CoTPP-cov**, a striking difference between immobilisation modes becomes apparent from the comparison of TOF values (Fig. 4a). At the

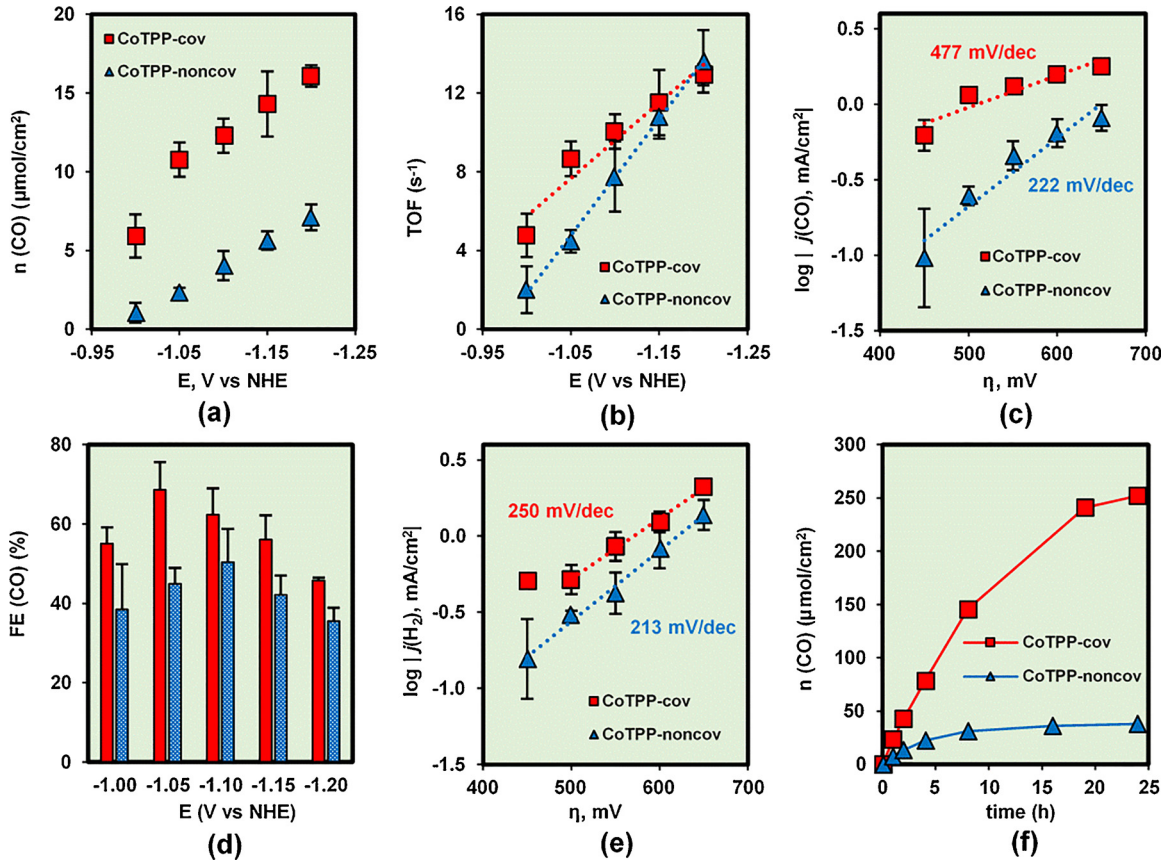

Fig. 4. (a) total amount of CO produced and (b) TOF observed for CoTPP in both immobilisation modes as a function of the applied potential; (c) Tafel plot of CO_2ERR; (d) FE (CO); (e) Tafel plot of H_2 evolution. Experiments were performed as 30 min runs in CO_2-saturated 0.5 M aqueous $KHCO_3$; measured values and standard deviation bars represent average of three measurements; (d) total amount of CO obtained during 24 h long electrolysis at -1.05 V vs NHE.

lowest studied potential of -1.00 V **CoTPP-cov** has TOF of 4.8 s^{-1} which is 2.4 times higher than that of **CoTPP-noncov**. However, at the potentials more negative than −1.10 V the difference in per site activity is less pronounced and TOF reaches 13 s^{-1} at -1.20 V in both cases. Clearly, covalent ligation of the catalyst to the carbon surface markedly increases CO_2ERR rate at low potentials.

To elucidate factors affecting the reaction speed, we plotted logarithm of average CO_2 reduction current density against overpotential (Fig. 4c). For **CoTPP-noncov**, Tafel plot has the slope of 222 mV/dec. This value is generally consistent with 255 mV/dec reported by Hu et al for CoTPP-CNT composite [32], but considerably higher than 165 mV/dec found for Co porphyrin embedded into MOF [35]. In strong contrast to **CoTPP-noncov**, for **CoTPP-cov** the slope is 477 mV/dec that is close to 470 mV/dec reported by Lin et al for CoTPP-based COF [38]. Also, current-overpotential relationship follows Ohm's law rather than the Tafel's and analysis of earlier works shows similar behavior for other macrocyclic catalysts containing Co atom.

One could clearly see that the kinetic behavior of **CoTPP-cov** and **CoTPP-noncov** are distinctively different. Although CO_2ERR is a complex multistep process [26,27], the following observations provide important clues: (i) Tafel plot steepness drops with the introduction of conjugated linker between porphyrin and electrode; (ii) TOF at the potentials close to reversible Co^I/Co^{II} redox couple substantially increases upon introduction of conductive linker (iii) CO evolution kinetics shows apparent deviation from logarithmic behavior coupled with the absence of curve flattening at high overpotentials. Clearly, the diffusion polarization could not be a limiting factor as otherwise the line flattening would be evident while purely electrochemical kinetics should lead to exponential rise of CO_2ERR curve [55]. Thus, we conclude that the CO formation reaction is fast compared to the speed of Co^ITPP species regeneration and the electron transfer onto the complex is a primary rate-limiting step at the potentials more positive than -1.10 V vs NHE. It appears that this process is responsible for the observed resistance polarization and π-system of phenylene anchoring group significantly improves Co^{II} to Co^I transformation. Meanwhile, more negative bias renders electron transfer from the electrode to the catalyst fast enough regardless of immobilisation mode and either CO extrusion or nucleophilic attack on CO_2 becomes the slowest process of catalytic cycle which manifests itself in merging of TOF curves (Fig. 4b).

FE (CO) is also dependent on the applied potential (Fig. 4d). The highest average FE (CO) of 67% for **CoTPP-cov** was achieved at −1.05 V. However, this value for **CoTPP-noncov** was only 50% at −1.10 V, i.e. at 50 mV more negative electrode bias. Regarding the dependence of FE (CO) on the electrode potential, two distinctively different mechanisms could lead to simultaneous formation of gases: both are produced solely on CoTPP or CO forms on the catalyst and H_2 on the support. Analysis of water discharge kinetics on **CoTPP-cov** and **CoTPP-noncov** reveals clear logarithmic dependence of the hydrogen evolution current on the potential (Figure S15). Tafel plots derived from these curves are rather parallel having slopes of 213 mV/dec for **CoTPP-cov** and 250 mV/dec for **CoTPP-noncov** (Fig. 4e). Although H^+ reduction measured on the bare carbon cloth has a slope of 105 mV/dec (Figure S14), this difference is expected considering that around half of the current is spent on CO_2ERR. Based on this, carbon fabric is responsible for concurrent H_2 production while CoTPP itself has selectivity to CO_2 of not less than 91% as measured by Hu et al. [32] Thus, FE (CO) is defined by superposition of H_2 evolution kinetics which is governed by exponential law and kinetics of CO_2ERR that is rather a function of the amount of accessible catalyst, its nature and the

Table 1
Comparison of heterogeneous metalloporphyrin catalysts operating in aqueous medium.

Entry	Catalyst	V vs NHE	Electrolyte	FE (CO), %	TOF, s^{-1}	Ref.
1	**CoTPP-cov**	−1.05	0.5 M $KHCO_3$	67	8.3	This work
2	**CoTPP-noncov**	−1.05	0.5 M $KHCO_3$	45	4.4	This work
3	CoTPP/CNT	−1.10	0.5 M $KHCO_3$	91	2.75	[32]
4	COF-367-Co	−1.09	0.5 M $KHCO_3$	91	0.56	[38]
5	COF-367-Co (1%)	−1.09	0.5 M $KHCO_3$	40	2.6	[38]
6	CAT_{Pyr}/CNT	−1.03	0.5 M $NaHCO_3$	93	0.04	[34]
7	CAT_{CO2H}	−1.06	0.5 M $NaHCO_3$	86	0.05	[40]

speed of electron transfer from the electrode surface onto catalytically active centre. Hence, the point of the highest FE (CO) corresponds to the balance where CO_2ERR is already fast and water discharge is still slow.

Finally, we studied long-term performance of CoTPP-modified electrodes under potential of -1.05 V vs NHE where **CoTPP-cov** showed the highest FE (CO). By the end of 24 h long electrolysis **CoTPP-cov** produced 252 μmol/cm^2 of CO as opposed to **CoTPP-noncov** with the overall CO production of 38 μmol/cm^2 (Fig. 4d). Cumulative TON of **CoTPP-cov** was calculated to be $3.9{\cdot}10^5$ while that of **CoTPP-noncov** was $1.3{\cdot}10^5$ only (Figure S17a). FE (CO) for **CoTPP-cov** reached 81% and the catalyst maintained high FE (CO) for at least 8 h (Figure S17b). Clearly, TON observed for **CoTPP-cov** was 3 times higher with better FE (CO) which means that covalent immobilization does improve overall stability of the electrode material. However, by the end of electrolysis FE (CO) and TOF dropped in both cases due to changes in porphyrin structure [32]. Based on these observations, we concluded that more than one mechanism is responsible for the catalyst deactivation. Strong bond with electrode surface does prevent such phenomena as leaching and recrystallisation while stability of the complex itself is largely unaffected by heterogenization mode.

Compared with earlier reports concerning CoTPP-based catalysts, TOF values obtained in our work both for **CoTPP-cov** and **CoTPP-noncov** (Table 1, entries 1 and 2) are clearly higher. As not all non-covalently deposited complex is electrochemically active, in case of CoTPP/CNT hybrid this difference is most likely due to the fact that we used Γ_{EA} values instead of total catalyst loading (Table 1, entry 3) [32]. In case of COFs the resulting TOF most probably is affected by CO_2 diffusion limitations within porous framework structure [38]. At the same time, estimation of surface loading for Fe counterparts was performed in the same manner and the catalytic activity of our **CoTPP-cov** is ~ 200 and ~ 160 times higher than that of CAT_{Pyr} and CAT_{CO2H} respectively (Table 1, entries 6 and 7) [34,40]. Although the average FE (CO) we measured in our work is somewhat lower than that described in previous reports, it is the result of carbon fabric being used as a support instead of CNTs.

4. Conclusion

In summary, we studied the effect of covalent ligation to carbon cloth on electrocatalytic activity of CoTPP in CO_2ERR in aqueous medium. Due to presence of π-conjugated linker between carbon electrode and CoTPP, TOF at overpotentials below 550 mV rose by the factor of ~2 compared to **CoTPP-noncov**. Moreover, surface density of electrochemically active species significantly increased and FE (CO) also reached the highest value at 50 mV less negative potential. As a result of simultaneous improvement in TOF and Γ_{EA}, **CoTPP-cov** produced 6.6 times more CO than noncovalently deposited counterpart in a 24 h long catalytic experiment with FE (CO) reaching 81%. Cumulative TON value of $3.9{\cdot}10^5$ is one of the highest reported to date. Electrokinetic data show that the phenylene linker enhances electron transfer rate from the electrode to porphyrin core functioning virtually as a conductive molecular wire while H_2 is produced on the carbon support. Thus, covalent immobilisation is a key element in overall design of efficient heterogeneous electrocatalysts for CO_2ERR.

Acknowledgement

Financial support by the ARC Discovery Project (DP14010243), ARC Discovery Early Career Researcher Award (DE120100329) and Macquarie University iMQRTP scholarship is gratefully acknowledged. Also, authors would like to thank Prof. Yves De Deene for access to NMR spectrometer, Australian Proteome Analysis Facility (APAF) for ESI MS analyses, Macquarie University Microscope Facility and Geoanalytical Electron Microscopy Facility for access to their instrumentation and staff.

Appendix A. Supplementary data

Supplementary material related to this article can be found, in the online version, at doi:https://doi.org/10.1016/j.apcatb.2018.11.084.

References

[1] M.T. Jensen, M.H. Rønne, A.K. Ravn, R.W. Juhl, D.U. Nielsen, X.-M. Hu, S.U. Pedersen, K. Daasbjerg, T. Skrydstrup, Scalable carbon dioxide electroreduction coupled to carbonylation chemistry, Nat. Comm. 8 (1) (2017) 489.
[2] J. Qiao, Y. Liu, F. Hong, J. Zhang, A review of catalysts for the electroreduction of carbon dioxide to produce low-carbon fuels, Chem. Soc. Rev. 43 (2) (2014) 631–675.
[3] N.S. Lewis, D.G. Nocera, Powering the planet: chemical challenges in solar energy utilization, Proc. Natl. Acad. Sci. 103 (43) (2006) 15729–15735.
[4] C. Mora, G.A. Frazier, J.R. Longman, S.R. Dacks, M.M. Walton, J.E. Tong, J.J. Sanchez, R.L. Kaiser, O.Y. Stender, M.J. Anderson, M.C. Ambrosino, I. Fernandez-Silva, M.L. Giuseffi, W.T. Giambelluca, The projected timing of climate departure from recent variability, Nature 502 (2013) 183–187.
[5] D.T. Whipple, P.J.A. Kenis, Prospects of CO_2 utilization via direct heterogeneous electrochemical reduction, J. Phys. Chem. Lett. 1 (24) (2010) 3451–3458.
[6] J.-M. Savéant, Molecular catalysis of electrochemical reactions. mechanistic aspects, Chem. Rev. 108 (7) (2008) 2348–2378.
[7] C. Costentin, M. Robert, J.-M. Saveant, Catalysis of the electrochemical reduction of carbon dioxide, Chem. Soc. Rev. 42 (6) (2013) 2423–2436.
[8] E.E. Benson, C.P. Kubiak, A.J. Sathrum, J.M. Smieja, Electrocatalytic and homogeneous approaches to conversion of CO2 to liquid fuels, Chem. Soc. Rev. 38 (1) (2009) 89–99.
[9] K. Jiang, R.B. Sandberg, A.J. Akey, X. Liu, D.C. Bell, J.K. Nørskov, K. Chan, H. Wang, Metal ion cycling of Cu foil for selective C–C coupling in electrochemical CO_2 reduction, Nat. Catal. 1 (2) (2018) 111–119.
[10] P. De Luna, R. Quintero-Bermudez, C.-T. Dinh, M.B. Ross, O.S. Bushuyev, P. Todorović, T. Regier, S.O. Kelley, P. Yang, E.H. Sargent, Catalyst electro-redeposition controls morphology and oxidation state for selective carbon dioxide reduction, Nat. Catal. 1 (2) (2018) 103–110.
[11] Y. Chen, M.W. Kanan, Tin oxide dependence of the CO_2 reduction efficiency on tin electrodes and enhanced activity for tin/tin oxide thin-film catalysts, J. Am. Chem. Soc. 134 (4) (2012) 1986–1989.
[12] M. Asadi, B. Kumar, A. Behranginia, B.A. Rosen, A. Baskin, N. Repnin, D. Pisasale, P. Phillips, W. Zhu, R. Haasch, R.F. Klie, P. Král, J. Abiade, A. Salehi-Khojin, Robust carbon dioxide reduction on molybdenum disulphide edges, Nat. Comm. 5 (2014) 4470.
[13] X. Lu, T.H. Tan, Y.H. Ng, R. Amal, Highly selective and stable reduction of CO_2 to CO by a graphitic carbon nitride/carbon nanotube composite electrocatalyst, Chem. Eur. J. 22 (34) (2016) 11991–11996.
[14] J. Wu, S. Ma, J. Sun, J.I. Gold, C. Tiwary, B. Kim, L. Zhu, N. Chopra, I.N. Odeh, R. Vajtai, A.Z. Yu, R. Luo, J. Lou, G. Ding, P.J.A. Kenis, P.M. Ajayan, A metal-free electrocatalyst for carbon dioxide reduction to multi-carbon hydrocarbons and oxygenates, Nat. Comm. 7 (2016) 13869.
[15] J. Wu, R.M. Yadav, M. Liu, P.P. Sharma, C.S. Tiwary, L. Ma, X. Zou, X.-D. Zhou, B.I. Yakobson, J. Lou, P.M. Ajayan, Achieving highly efficient, selective, and stable

CO2 reduction on nitrogen-doped carbon nanotubes, ACS Nano 9 (5) (2015) 5364–5371.
[16] I. Azcarate, C. Costentin, M. Robert, J.-M. Savéant, Through-space charge interaction substituent effects in molecular catalysis leading to the design of the most efficient catalyst of CO_2-to-CO electrochemical conversion, J. Am. Chem. Soc. 138 (51) (2016) 16639–16644.
[17] C. Costentin, S. Drouet, M. Robert, J.-M. Savéant, A local proton source enhances CO_2 electroreduction to CO by a molecular Fe catalyst, Science 338 (6103) (2012) 90–94.
[18] E.A. Mohamed, Z.N. Zahran, Y. Naruta, Efficient electrocatalytic CO_2 reduction with a molecular cofacial iron porphyrin dimer, Chem. Comm. 51 (95) (2015) 16900–16903.
[19] R.B. Ambre, Q. Daniel, T. Fan, H. Chen, B. Zhang, L. Wang, M.S.G. Ahlquist, L. Duan, L. Sun, Molecular engineering for efficient and selective iron porphyrin catalysts for electrochemical reduction of CO_2 to CO, Chem. Comm. 52 (100) (2016) 14478–14481.
[20] Y. Wu, J. Jiang, Z. Weng, M. Wang, D.L.J. Broere, Y. Zhong, G.W. Brudvig, Z. Feng, H. Wang, Electroreduction of CO_2 catalyzed by a heterogenized Zn–porphyrin complex with a redox-innocent metal center, ACS Central Sci. 3 (8) (2017) 847–852.
[21] C. Costentin, M. Robert, J.-M. Savéant, A. Tatin, Efficient and selective molecular catalyst for the CO_2-to-CO electrochemical conversion in water, Proc. Natl. Acad. Sci. 112 (22) (2015) 6882–6886.
[22] D. Behar, T. Dhanasekaran, P. Neta, C.M. Hosten, D. Ejeh, P. Hambright, E. Fujita, Cobalt porphyrin catalyzed reduction of CO_2. Radiation chemical, photochemical, and electrochemical studies, J. Phys. Chem. A 102 (17) (1998) 2870–2877.
[23] J. Grodkowski, D. Behar, P. Neta, P. Hambright, Iron porphyrin-catalyzed reduction of CO_2. Photochemical and radiation chemical studies, J. Phys. Chem. A 101 (3) (1997) 248–254.
[24] J. Grodkowski, T. Dhanasekaran, P. Neta, P. Hambright, B.S. Brunschwig, K. Shinozaki, E. Fujita, Reduction of cobalt and iron phthalocyanines and the role of the reduced species in catalyzed photoreduction of CO_2, J. Phys. Chem. A 104 (48) (2000) 11332–11339.
[25] J. Grodkowski, P. Neta, E. Fujita, A. Mahammed, L. Simkhovich, Z. Gross, Reduction of cobalt and iron corroles and catalyzed reduction of CO_2, J. Phys. Chem. A 106 (18) (2002) 4772–4778.
[26] I.M.B. Nielsen, K. Leung, Cobalt − Porphyrin catalyzed electrochemical reduction of carbon dioxide in water. 1. A density functional study of intermediates, J. Phys. Chem. A 114 (37) (2010) 10166–10173.
[27] K. Leung, I.M.B. Nielsen, N. Sai, C. Medforth, J.A. Shelnutt, Cobalt − porphyrin catalyzed electrochemical reduction of carbon dioxide in water. 2. Mechanism from first principles, J. Phys. Chem. A 114 (37) (2010) 10174–10184.
[28] C. Römelt, J. Song, M. Tarrago, J.A. Rees, M. van Gastel, T. Weyhermüller, S. DeBeer, E. Bill, F. Neese, S. Ye, Electronic structure of a formal Iron(0) porphyrin complex relevant to CO_2 reduction, Inorg. Chem. 56 (8) (2017) 4745–4750.
[29] A.J. Göttle, M.T.M. Koper, Determinant role of electrogenerated reactive nucleophilic species on selectivity during reduction of CO_2 catalyzed by metalloporphyrins, J. Am. Chem. Soc. 140 (14) (2018) 4826–4834.
[30] C.L. Yao, J.C. Li, W. Gao, Q. Jiang, Cobalt-porphine catalyzed CO_2 electro-reduction: a novel protonation mechanism, Phys. Chem. Chem. Phys. 19 (23) (2017) 15067–15072.
[31] C. Costentin, M. Robert, J.-M. Savéant, Molecular catalysis of electrochemical reactions, Curr. Opin. Electrochem. 2 (1) (2017) 26–31.
[32] X.-M. Hu, M.H. Rønne, S.U. Pedersen, T. Skrydstrup, K. Daasbjerg, Enhanced catalytic activity of cobalt porphyrin in CO_2 electroreduction upon immobilization on carbon materials, Angew. Chem. 129 (23) (2017) 6568–6572.
[33] X. Zhang, Z. Wu, X. Zhang, L. Li, Y. Li, H. Xu, X. Li, X. Yu, Z. Zhang, Y. Liang, H. Wang, Highly selective and active CO_2 reduction electrocatalysts based on cobalt phthalocyanine/carbon nanotube hybrid structures, Nat. Comm. 8 (2017) 14675.
[34] A. Maurin, M. Robert, Noncovalent immobilization of a molecular iron-based electrocatalyst on carbon electrodes for selective, efficient CO_2-to-CO conversion in water, J. Am. Chem. Soc. 138 (8) (2016) 2492–2495.
[35] N. Kornienko, Y. Zhao, C.S. Kley, C. Zhu, D. Kim, S. Lin, C.J. Chang, O.M. Yaghi, P. Yang, Metal–organic frameworks for electrocatalytic reduction of carbon dioxide, J. Am. Chem. Soc. 137 (44) (2015) 14129–14135.
[36] I. Hod, M.D. Sampson, P. Deria, C.P. Kubiak, O.K. Farha, J.T. Hupp, Fe-porphyrin-based metal–organic framework films as high-surface concentration, heterogeneous catalysts for electrochemical reduction of CO_2, ACS Catal. 5 (11) (2015) 6302–6309.
[37] C.S. Diercks, S. Lin, N. Kornienko, E.A. Kapustin, E.M. Nichols, C. Zhu, Y. Zhao, C.J. Chang, O.M. Yaghi, Reticular electronic tuning of porphyrin active sites in covalent organic frameworks for electrocatalytic carbon dioxide reduction, J. Am. Chem. Soc. 140 (3) (2018) 1116–1122.
[38] S. Lin, C.S. Diercks, Y.-B. Zhang, N. Kornienko, E.M. Nichols, Y. Zhao, A.R. Paris, D. Kim, P. Yang, O.M. Yaghi, C.J. Chang, Covalent organic frameworks comprising cobalt porphyrins for catalytic CO2 reduction in water, Science 349 (6253) (2015) 1208–1213.
[39] X.-M. Hu, Z. Salmi, M. Lillethorup, E.B. Pedersen, M. Robert, S.U. Pedersen, T. Skrydstrup, K. Daasbjerg, Controlled electropolymerisation of a carbazole-functionalised iron porphyrin electrocatalyst for CO_2 reduction, Chem. Comm. 52 (34) (2016) 5864–5867.
[40] A. Maurin, M. Robert, Catalytic CO_2-to-CO conversion in water by covalently functionalized carbon nanotubes with a molecular iron catalyst, Chem. Comm. 52 (81) (2016) 12084–12087.
[41] S.A. Yao, R.E. Ruther, L. Zhang, R.A. Franking, R.J. Hamers, J.F. Berry, Covalent attachment of catalyst molecules to conductive diamond: CO_2 reduction using “Smart” electrodes, J. Am. Chem. Soc. 134 (38) (2012) 15632–15635.
[42] N. Elgrishi, S. Griveau, M.B. Chambers, F. Bedioui, M. Fontecave, Versatile functionalization of carbon electrodes with a polypyridine ligand: metallation and electrocatalytic H^+ and CO_2 reduction, Chem. Comm. 51 (14) (2015) 2995–2998.
[43] P. Allongue, M. Delamar, B. Desbat, O. Fagebaume, R. Hitmi, J. Pinson, J.-M. Savéant, Covalent modification of carbon surfaces by aryl radicals generated from the electrochemical reduction of diazonium salts, J. Am. Chem. Soc. 119 (1) (1997) 201–207.
[44] J. He, Q. Fu, S. Lindsay, J.W. Ciszek, J.M. Tour, Electrochemical origin of voltage-controlled molecular conductance switching, J. Am. Chem. Soc. 128 (46) (2006) 14828–14835.
[45] G. Gritzner, J. Kůta, Recommendations on reporting electrode potentials in non-aqueous solvents: IUPC commission on electrochemistry, Electrochim. Acta 29 (6) (1984) 869–873.
[46] J.-M. Savéant, Elements of Molecular and Biomolecular Electrochemistry, John Wiley & Sons, Inc., 2006, pp. 1–77.
[47] S. Baranton, D. Bélanger, Electrochemical derivatization of carbon surface by reduction of in situ generated diazonium cations, J. Phys. Chem. B 109 (51) (2005) 24401–24410.
[48] S. Mahouche-Chergui, S. Gam-Derouich, C. Mangeney, M.M. Chehimi, Aryl diazonium salts: a new class of coupling agents for bonding polymers, biomacromolecules and nanoparticles to surfaces, Chem. Soc. Rev. 40 (7) (2011) 4143–4166.
[49] A.J. Gross, C. Bucher, L. Coche-Guerente, P. Labbé, A.J. Downard, J.-C. Moutet, Nickel (II) tetraphenylporphyrin modified surfaces via electrografting of an aryldiazonium salt, Electrochem. Comm. 13 (11) (2011) 1236–1239.
[50] M. Picot, I. Nicolas, C. Poriel, J. Rault-Berthelot, F. Barrière, On the nature of the electrode surface modification by cathodic reduction of tetraarylporphyrin diazonium salts in aqueous media, Electrochem. Comm. 20 (2012) 167–170.
[51] R.D. Rocklin, R.W. Murray, Chemically modified carbon electrodes: part XVII. Metallation of immobilized tetra(aminophenyl)porphyrin with manganese, iron, cobalt, nickel, copper and zinc, and electrochemistry of diprotonated tetraphenylporphyrin, J. Electroanal. Chem. Interfacial Electrochem. 100 (1) (1979) 271–282.
[52] Y.-C. Liu, R.L. McCreery, Reactions of organic monolayers on carbon surfaces observed with unenhanced Raman spectroscopy, J. Am. Chem. Soc. 117 (45) (1995) 11254–11259.
[53] F. Anariba, U. Viswanathan, D.F. Bocian, R.L. McCreery, Determination of the structure and orientation of organic molecules tethered to flat graphitic carbon by ATR-FT-IR and Raman spectroscopy, Anal. Chem. 78 (9) (2006) 3104–3112.
[54] C. Saby, B. Ortiz, G.Y. Champagne, D. Bélanger, Electrochemical modification of glassy carbon electrode using aromatic diazonium salts. 1. Blocking effect of 4-Nitrophenyl and 4-Carboxyphenyl groups, Langmuir 13 (25) (1997) 6805–6813.
[55] M. Stern, A.L. Geary, Electrochemical polarization I. A theoretical analysis of the shape of polarization curves, J. Electrochem. Soc. 104 (1) (1957) 56–63.